TRPM2 sensitizes to oxidative stress but attenuates high temperature injury in the sea anemone *Nematostella vectensis*

Wiebke Ehrlich[1], James M. Gahan[2], Fabian Rentzsch[2], Frank J.P. Kühn[3,*]

[1]Institute of Physiology, Medical Faculty, University hospital Aachen, Germany
[2]Sars International Centre for Marine Molecular Biology, University of Bergen., Norway
[3]University Hospital Aachen: Universitatsklinikum Aachen-University hospital, Aachen Pauwelsstr. 30, 52074 Aachen, Germany

[*]Author for correspondence: fkuehn@ukaachen.de

In humans, the cation channel TRPM2 (HsTRPM2) has been intensively studied because it is involved in oxidative stress mediated apoptosis and also contributes to temperature regulation. The gating mechanism of TRPM2 is quite complex where a C-terminally localized enzyme domain plays a crucial role. The analysis of orthologues of TRPM2, in particular from the distantly related marine invertebrate *Nematostella vectensis* (NvTRPM2) revealed that during evolution the functional role of the endogenous enzyme domain of TRPM2 has undergone fundamental changes. In this study we investigate whether these evolutionary differences also apply to the physiological functions of TRPM2. For this purpose, we generated a TRPM2 loss-of-function mutation in *Nematostella* and compared the phenotypes of wild-type and mutant animals after exposure to either oxidative stress or high temperature. Our results show that under standard culture conditions mutant animals are indistinguishable from wild-type animals in terms of morphology, and development. However, exposure of both experimental groups to different stressors revealed that TRPM2 sensitizes to oxidative stress but attenuates high temperature injury in *Nematostella*. Therefore, NvTRPM2 plays opposite roles in the cellular response to these two different stressors. These findings reveal a similar physiological spectrum of activity of TRPM2 in humans and *Nematostella* and open up the possibility to establish *Nematostella* as a model organism for the physiological function of TRPM2.

Introduction

The starlet sea anemone *Nematostella vectensis* has become a prominent model system for genomic and developmental studies (e.g., Layden et al., 2016; Darling et al., 2005). This is mainly due to the fact that, despite the long evolutionary distance, vertebrates and sea anemones retain a striking degree of similarity in gene repertoire and intron/exon structure (Technau et al., 2005; Sullivan et al., 2006; Putnam et al., 2007). Furthermore, these two metazoan groups share many signalling pathways that regulate e.g., development (Technau et al., 2005) and innate immunity (Miller et al., 2007). The natural habitat of *Nematostella* is shallow and brackish water zones of the Atlantic and Pacific coast of North America and of the south and east coast of England (Sheader and Rowe, 1997). The environmental conditions in these habitats are highly variable, exposing *Nematostella* to strong environmental stressors including changes in temperature, salinity, ultraviolet radiation, and levels of reactive oxygen species (Uhlinger et al., 1992; Sheader and Rowe, 1997). This is especially true for the contemporary degradation of these habitats due to anthropogenic impacts (Harter and Matthews, 2005). It is therefore tempting to consider *Nematostella* also as a marine invertebrate model system for the response of multicellular organisms to environmental stress (Reitzel et al., 2008; Elran et al., 2014; Tarrant et al., 2014).

The physiological tolerance of an organism is determined by its repertoire of stress response genes. Comparative genetic studies on diverse organisms have revealed that many components of the stress response network are conserved between bilaterians and *Nematostella*, among them genes involved in the responses to oxidative stress (Reitzel et al., 2008). In humans, the cellular responses induced by oxidative stress have been intensively studied, as they often represent the starting point for numerous pathophysiological processes (e.g., Malko & Jiang, 2020). This specifically includes cellular apoptosis triggered by oxidative stress, which is mediated by the nicotinamide adenine dinucleotide (NAD^+) metabolite adenosine diphosphate ribose (ADPR; Fonfria et al., 2004; Perraud et al., 2005). It has been shown that in human cells oxidative stress induces intracellular pathways leading to poly-ADP-ribosylation of DNA and various nuclear proteins. This process is catalysed by the enzyme Poly-ADPR Polymerase type 1 (PARP-1). Subsequently, Poly-ADPR-Glycohydrolase (PARG) degrades the poly-ADPR chains to monomeric ADPR (e.g., reviewed in Pascal and Ellenberger, 2015). The resulting increase in the cytosolic ADPR concentration in turn leads to the direct activation of the ADPR-dependent transient receptor potential melastatin type 2 (TRPM2) channel (Perraud et al., 2001, 2005). The binding of ADPR to this non-selective plasma membrane cation channel causes a massive influx of

calcium through the channel pore, which in most cases leads to cell death. This indirect activation of HsTRPM2 by oxidative stress can be experimentally simulated by extracellular application of H_2O_2 (Hara et al., 2002).

A unique feature of TRPM2 is the presence of a C-terminal domain, which is homologous to the human ADPR diphosphatase NUDT9 (Perraud et al., 2001). Initially it was postulated that this domain plays the crucial role in the ADPR-dependent activation of TRPM2 (e.g., reviewed in Kühn, 2020). In this regard, however, a paradigm shift recently occurred, since comparative in *vitro* analyses of TRPM2 orthologues, in particular that of *Nematostella* (NvTRPM2), revealed that the activation of TRPM2 by ADPR also works without the NUDT9 homology (NUDT9H) domain (Kühn et al., 2016, 2017). Moreover, an additional ADPR binding pocket in the N-terminal part of TRPM2 has been recently confirmed by cryogenic electron microscopy (Huang et al., 2018, 2019). In the human TRPM2 orthologue, the NUDT9H domain has no enzymatic activity but is indispensable for pore opening (Perraud et al., 2001, 2003; Kühn et al., 2016; Iordanov et al., 2016), whereas in NvTRPM2 NUDT9H has full ADPRase activity but does not affect channel function (Kühn et al., 2016; Iordanov et al., 2019).

Besides its prominent role in oxidative stress mediated apoptosis, in mammals TRPM2 is involved in numerous physiological processes such as immune cell activation (Yamamoto et al., 2008), insulin secretion (Uchida et al., 2011) and innate immunity (Knowles et al., 2013). In humans TRPM2 was also shown to regulate core body temperature (Tan and McNaughton, 2016; Song et al., 2016). Interestingly, there is experimental evidence that oxidative stress (H_2O_2) sensitizes mouse TRPM2 to higher temperatures (Tan and McNaughton, 2016). The interplay of oxidative stress and increased temperature is also of great relevance for the ecology of marine invertebrates. This is particularly true for coral bleaching, which is closely associated with oxidative stress and higher temperatures ref. to e.g. Downs et al. 2002 and Dias et al. 2019. In this regard, TRPM2 would represent a promising target to investigate the underlying molecular mechanism in more detail.

Investigations on cellular factors dealing with oxidative stress have been already performed in diverse cnidarians among them *Nematostella*. In one study several antioxidant enzymes of the superoxide dismutase family could be identified in *Nematostella*, and changes in their expression profile were detected after exposure to UV-radiation, crude oil and polycyclic aromatic hydrocarbons (Tarrant et al., 2014). A further study revealed differences in peroxide sensitivity between and within populations of *Nematostella* (Friedmann et al., 2018).

In this study we aimed to gain first insights into the physiological importance of TRPM2 in *Nematostella* by generating a loss-of-function mutant. We investigated whether this cation channel in *Nematostella* is also involved in the response to oxidative stress or in the sensitivity to high temperature, despite the clear differences compared to the human orthologue with regard to the gating mechanism.

Our data reveal that in *Nematostella*, TRPM2 mediates tissue damage after exposure to oxidative stress (H_2O_2) but attenuates tissue damage after exposure to elevated (38.9°C) temperatures. These results suggest that TRPM2 plays a similar role in humans and *Nematostella* with respect to the response to oxidative stress. In case of the responses to high-temperature stress, TRPM2 seems to have a protective function in *Nematostella*. Thus, a direct connection between higher temperatures and oxidative stress cannot be reconciled with the functional role of TRPM2 in *Nematostella*.

Experimental procedures

***Nematostella* culture.** Rearing, spawning and induction of regeneration of *Nematostella* individuals was performed following the protocol of Stefanik et al. (2013).

Preparation of tissue lysates from sea anemones. Adult animals of *Nematostella* were relaxed in 7 mM $MgCl_2$ dissolved in *Nematostella* medium (NM, 1/3 artificial sea water; Instant Ocean). A piece of tissue a few millimeters in size of different animals (head and physa) were dissected. The animals were pushed to the ground of a petri dish using a razorblade and tissue was dissected by cutting along the razorblade with a scalpel. For each sample that was analysed the tissue of six different animals (three heads and three physae) was pooled. The sampled tissues were washed with PBS before an adequate volume of CelLytic MT Lysisbuffer (50 mg tissue sample in 1000 µl lysis buffer) (Sigma-Aldrich, St. Louis, USA) containing 1 % protease inhibitor (Sigma-Aldrich, St. Louis, USA) was added. The tissue was sheared using scissors and dissociated by five 1 sec sonification steps at power level two (Branson Sonifier 150, Heinemann, Schwäbisch Gmünd, Germany). After incubation for 15 min on ice, in which the samples were vortexed for 5 sec every 5 min two additional sonification steps were performed before the samples were centrifuged at 12.000 x g for 15 min at 4°C. The clarified supernatant was transferred to a new tube and protein concentration was measured by Bradford reagent (Thermo Fisher Scientific, Waltham, USA)

according to the manufacturer's instructions. The lysates were stored at -20°C until further analysed by SDS-PAGE gel electrophoresis and Western blot analysis.

Generation of *TRPM2* loss-of-function mutants in *Nematostella*. Mutants were generated using a CRSPR-Cas9-mediated mutagenesis approach as previously published (Ikmi et al., 2014; Kraus et al., 2016). A single guide RNA (sgRNA) species was designed to target the genome region representing the central part of the pore domain of NvTRPM2. The sgRNA was synthesized using the EnGen™ sgRNA Synthesis Kit, *S. pyogenes* (New England Biolabs, Ipswich, USA) according to the manufacturer's instructions. For this purpose, the target-specific oligonucleotide (5'-TTCTAATACGACTCACTATAGGGCGGTGTTCACGATCGCGTAGTTTTAGAGCTAG A-3') was designed according to the manufacturer's instructions of EnGen™ sgRNA Synthesis Kit, *S. pyogenes*, and synthesized by Sigma-Aldrich (Missouri, USA). Fertilized eggs of *Nematostella* were dejellied with 1 % cysteine (Sigma-Aldrich, Missouri, USA) dissolved in NM by shaking for 15 min. The dejellied eggs were then washed seven times in NM. The injection mix (Cas9 endonuclease [1 mg/ml] / Alexa fluorescent dye dissolved in 1.1 M KCl / sgRNA 450 ng / H_2O up to total volume of 4 µl) was prepared and pre-warmed for 5 min to 37°C. Microinjection was performed using a Femtojet microinjector on a Nikon TE2000-S inverted microscope until the first cleavages of the eggs occur. The injected animals (F_0 generation) were grown to sexual maturity and crossed to wild-type animals to obtain a heterozygous F_1 generation. These animals were screened by genomic sequencing for the presence of NvTRPM2 mutations. Female and male animals containing the same mutation of NvTRPM2 were crossed to generate homozygous NvTRPM2 knockout animals (F_2 generation). These animals were screened by genomic sequencing and for further analysis separated according to their NvTRPM2 genotype (homozygous wildtype, heterozygous mutant, homozygous mutant). The mutant *NvTRPM2* allele used in this study was designated $NvTRPM2^{1016Stop}$ (see Results for explanation)

Extraction, purification and sequencing of genomic DNA. Tissue of the putatively mutated animals was dissected, and extraction of the genomic DNA was performed by addition of 200 µl Ethanol (100 %), vortexing and incubation for 5 min. After a short centrifugation step in a table centrifuge at 6000 g, the supernatant was discarded, and the sample pellet was dried with open lid for 45 min at 50°C in a PCR machine. Subsequently 20 to 50 µl of yDNA buffer (10 mM TrisHCl / 1 mM EDTA / 25 mM NaCl) supplemented with freshly prepared proteinase K

(200 µg/µl; New England Biolabs, Ipswich, USA) were added. The mixture was vortexed and incubated for 2 hrs at 50°C and then 10 min at 98°C. Thereafter, the samples were briefly centrifuged in a table centrifuge (6000 g) and the supernatant containing the genomic DNA was transferred to a new tube and stored at -20°C. The DNA region of the genome targeted by CRISPR-Cas9/sgRNA was amplified by PCR using a sense and an antisense primer which bind upstream and downstream of the target region, respectively. The following primers were synthesized (Sigma Aldrich, Missouri, USA): Forward (sense) primer: (5'-CGCTCGTGGTGTGTGTTC-TAAC-3'); reverse (antisense) primer: (5'-GTCGAATCAGCGCACGAGATTCAC-3'). For PCR, the Q5 high-fidelity PCR kit (New England Biolabs, Ipswich, USA) was used according to the manufacturer's instructions. The temperature protocol included initial denaturation for 1 min at 98°C, followed by 40 cycles with a denaturation step for 15 sec at 98°C, annealing step for 30 sec at 72°C and extension step for 150 sec at 72°C. After final extension for 10 min at 72°C the PCR product was cooled to 4°C. For purification, the PCR product was subjected to agarose (0.8 %) gel electrophoresis and the expected DNA fragment was isolated by gel extraction (QIAquick Gel Extraction Kit, Qiagen, Hilden, Germany) according to the manufacturer's instructions. The purified DNA fragment was sequenced using the original PCR forward primer (Sigma Aldrich, Missouri, USA).

Molecular cloning, cell culture and transfection. The cDNA of *Nematostella TRPM2 (NvTRPM2)* with codon usage adapted for heterologous expression in human cells was sub cloned as previously described (Kühn et al., 2015). Site-directed mutagenesis (QuikChange mutagenesis system, Agilent, Santa Clara, USA) was performed according to the manufacturer's instructions in order to reproduce the NvTRPM2^{1016Stop}mutation for in *vitro* analysis. For immunohistological analysis in control experiments of Western-blots or biotinylation assays, variants of wild-type *NvTRPM2* and NvTRPM2^{1008Stop} were generated which contain a triple hemagglutinin (3xHA)-tag at the C-terminus (previously described in Kühn et al., 2016). All mutations and sequence manipulations were verified by DNA sequencing (Eurofins Scientific, Luxembourg, Luxembourg)**.** Human embryonic kidney (HEK-293) cells were obtained from the German Collection of Microorganisms and Cell Cultures (Braunschweig, Germany) and regular authenticated as well as tested for contamination. Cell culture and heterologous expression of NvTRPM2 or NvTRPM2^{1008Stop} channels in HEK-293 cells using transient transfection of the corresponding cDNA was performed as previously described (Kühn et al., 2019).

Cell surface biotinylation and Western-blot analysis. The biotinylation assays and Western blots of heterologously transfected HEK-cells were performed as described previously (Kühn et al., 2019). For preparation of the membrane fraction from cell material of *Nematostella vectensis* we used a differential centrifugation protocol previously established by Vriens et al. (2005). A primary monoclonal mouse-anti-HA-tag (1:1000; cat.no. H3663; Sigma-Aldrich, USA) and mouse-anti-β-actin (1:1000; cat.no. 8H10D10; Cell-Signaling, USA) were used in combination with a rabbit-anti-mouse-HRP conjugated secondary antisera (1:1000; cat.no. P0261; DAKO, Agilent, USA). For Western blot analysis of NvTRPM2 expression in *vitro*, different monoclonal rabbit-anti-NvTRPM2 antisera (1:100; Davids Biotechnology, Regensburg, Germany) were used. The antiserum designated as "type N2" was directed against the N-terminus specific epitope (EDEVRAKVVEVFGAKGADK) of the NvTRPM2 protein. For Western blot analysis of NUDT9 expression in *vivo*, a mouse-anti-human-NUDT9 antiserum (1:500; cat.no. TA503235; Origene, Rockville, USA) was used. As secondary antisera either swine-anti-rabbit-HRP (1:1000; cat.no. P0217; DAKO, Agilent, Santa Clara, USA) or rabbit-anti-mouse-HRP (1:1000; cat.no. P0261; DAKO, Agilent, Santa Clara, USA) conjugated antisera were used. Detection of the HRP conjugated secondary antisera was performed using Intas Infinity ECL Starlight (Intas Science Imaging Instruments, Göttingen, Germany) and ChemoStar Touch (Intas Science Imaging Instruments, Göttingen, Germany) imaging system.

Electrophysiology. HEK-293 cells, heterologous expressing wild-type NvTRPM2 (control) or NvTRPM2^{1008Stop} channel variant, were stimulated with ADPR and Ca^{2+} and examined by whole-cell patch-clamp analysis as already described elsewhere (Kühn et al., 2019).

Immunofluorescence confocal microscopy. Embryos (blastula to 4-tentacle-polyp stage) were relaxed in 7 mM $MgCl_2$ in NM for 10 min and fixed for 30 min in ice cold Lavdovsky Fixative (50 % Ethanol / 3.7 % Paraformaldehyde / 4 % acetic acid / H_2O) at 4°C. The animals were washed three times for 10 min, first in 0.1 % Tween20 / PBS, then in 0.1 % Triton x-100 / 0.1 % Tween20 / PBS and finally in 0.1 % Tween20 / PBS on a shaker at room temperature (RT). The embryos were incubated overnight at 4°C with our N-terminus specific rabbit-anti-NvTRPM2-antiserum "type N2" (as described above) 1:200 diluted in 0.5 % skim milk powder / 0.1 % Tween20 / PBS. After three washing steps for 10 min in 0.1 % Tween20 / PBS, the embryos were incubated for 2.5 hrs at RT in the dark with a goat-anti-rabbit secondary antiserum coupled to an Alexa 488 fluorescent dye (1:400 diluted in 0.5 % skim

milk powder / 0.1 % Tween20 / PBS; cat.no. A11034; DAKO, Agilent, Santa Clara, USA). Finally, embryos were incubated for 5 min at RT in the dark with Hoechst (1:10,000 diluted from stock solution 1 µg/ml in PBS; Thermo Fisher Scientific, Waltham, USA) and mounted on glass slides using Fluoromount-G mounting solution (SouthernBiotech, Birmingham, USA). For imaging a Zeiss LSM 700 confocal microscope (software version ZEN 2011 SP7 FP3) was used.

Temporary treatment with H_2O_2. Individual 4-tentacle-polyps of wildtype and NvTRPM2^{1016Stop} animals were transferred in single wells of 6-well-plates. The animals were incubated with 0.00025 % H_2O_2 in NM for 5 hrs at standard culture conditions (18°C in the dark). Then, H_2O_2 was washed out with standard medium, and the animals were returned to standard culture conditions. As negative controls, wildtype and NvTRPM2^{1016Stop} 4-tentacle-polyps were treated in the same manner but without H_2O_2 treatment. The 4-tentacle-polyps were held in a relaxed state by incubation with 7 mM $MgCl_2$ in NM and bright-field images were taken, using a Nikon Eclipse Ts2 microscope and a Nikon DS-Fi3 camera at the following time points: Before and 1, 2, 3 and 15 days after H_2O_2 treatment. Different degrees of tissue damage were observed after H_2O_2 treatment and further analysed by Phalloidin staining (as described below), in order to identify effects on the muscle system. By evaluating the observed effects on overall morphology and integrity of the muscular system, we established two different categories, detailed within the results, and distinguish between "mild" and "severe" tissue damage.
The treated animals were classified in the different categories and the frequency of animals displaying mild or severe tissue damage was compared between wildtype and NvTRPM2^{1016Stop} animals. Six animals of each genotype were examined in each experiment, and a total of ten of such experiments were performed (altogether 60 animals of each genotype were analysed).

Temporary exposure to high temperatures. The experimental design was similar to that used for the treatment with H_2O_2. 4-tentacle-polyps of wildtype and NvTRPM2^{1016Stop} animals were transferred in 0.2 ml PCR tubes and incubated at 38.9°C for 6 hrs in a PCR machine. Then, the animals were returned to standard culture conditions. As negative controls, wildtype and NvTRPM2^{1016Stop} 4-tentacle-polyps were treated in the same manner but without high temperature treatment. The animals were relaxed with 7 mM $MgCl_2$ in NM and bright-field images were taken before and 1, 2, 3 and 15 days after high-temperature treatment. If

compared to H_2O_2 treatment, the bright-field images and Phalloidin stainings of the high-temperature-treated animals showed similar degrees of tissue damage. Therefore, the same categories of tissue damage were applied to compare the effects of high-temperature treatment between wildtype and NvTRPM2^{1016Stop} animals. Six animals of each genotype were examined in each experiment, and a total of ten of such experiments were performed (altogether 60 animals of each genotype were analysed).

Phalloidin Staining. Animals displaying different categories of tissue damage after treatment with H_2O_2, or high temperature were analysed by Phalloidin staining to identify effects on the muscle system. For this purpose, treated animals as well as control animals of wildtype and NvTRPM2^{1016Stop} were relaxed in 7 mM $MgCl_2$ dissolved in NM and fixed overnight at 4°C in ice cold fixing solution (3.7 % paraformaldehyde / 0.1 % Tween20 / PBS). The next day, the samples were washed in PBTx (0.2 % Triton x-100 / PBS) for 2 hrs. Every 0.5 hrs the washing solution was exchanged. Then, the samples were incubated overnight at 4°C in the dark in Alexa Flour 555 Phalloidin (1:100 in PBTx, from 66 µM stock solution; Invitrogen, Thermo Fisher Scientific, Waltham, USA). After three washing steps each for 5 min in PBTx the DNA of the samples was stained for 5 min at room temperature in the dark by incubation with Hoechst 33342 (1:1000 from 1 µg/ml stock solution in PBTx; Thermo Fisher Scientific, Waltham, USA). The samples were washed two times for 10 min in PBTx and mounted on glass slides using Fluoromount-G mounting solution (SouthernBiotech, Birmingham, USA). Finally, the slides were dried at room temperature overnight in the dark and stored at 4°C. Imaging was performed with a Zeiss LSM 700 confocal microscope (software version ZEN 2011 SP7 FP3).

Data analysis and statistics. The data of H_2O_2 and high-temperature stress tests were analysed using the GraphPad PRISM software and are expressed as the mean ± s.e.m. Statistical comparisons were performed using a two-way ANOVA and Fisher's LSD post-hoc test. Differences were considered significant at $^*P < 0.005$.

Results

Generation of *TRPM2* mutants in *Nematostella*

To study the physiological role of NvTRPM2 in *vivo*, an NvTRPM2 mutant was generated in *Nematostella* using the CRISPR-Cas9-mutagenesis method. We designed an sgRNA targeting the central part of the pore domain of *NvTRPM2* **(Fig. 1, A)**. The CRISPR-Cas9/sgRNA-

injected animals (F_0 generation) were grown to sexual maturity and crossed with wild-type animals. Genomic DNA-sequencing of tissue from individuals of the F_1 generation confirmed the presence of a two base pair deletion inducing a frameshift mutation at the target site and two premature stop codons in the downstream open reading frame **(Fig. 1, B).** As a result, the truncated channel variant should neither have an intact pore nor downstream protein sequences, and therefore most likely should be non-functional. We refer to this allele as *NvTRPM2*^{1016Stop}, indicating the predicted premature termination of translation after amino acid 1016.

In a next step, F_1 animals with the corresponding (-2 bp) frameshift mutation were crossed to generate F_2 offspring. Tissue from the resulting F_2 animals again was subjected to genotyping and revealed the whole spectrum of possible genotypes with homozygous wild-type as well as heterozygous and homozygous *NvTRPM2*^{1016Stop} mutants. Homozygous *NvTRPM2*^{1016Stop} mutants were viable and did not show any obvious morphological differences compared to wild-type polyps (see below). The F_2-offspring were sorted according to their *NvTRPM2* genotype and cultured for further analysis.

Heterologous expression of *Nematostella* wild-type TRPM2 and TRPM2^{1008Stop} variant in HEK-293 cells

Since no functional analysis method for the characterization of TRP channels in marine invertebrates has been established so far, we decided to test the effects of the NvTRPM2^{1016Stop} mutation in *Nematostella* by comparative phenotypic analysis of intact animals rather than by patch-clamp analysis or Calcium imaging of single cells. For the characterization of NvTRPM2^{1016Stop} in *vitro*, we tested surface expression as well as channel function using an established heterologous expression system of NvTRPM2 (Kühn et al., 2015). For this purpose, the corresponding frameshift mutation of the *NvTRPM2*^{1016Stop} allele was reproduced in *vitro* by site-directed mutagenesis **(Fig. 1, C)** of an *NvTRPM2* cDNA and analysed in comparison to wild-type NvTRPM2 in HEK-293 cells. For heterologous expression in HEK-293 cells the codon usage of the synthesized open reading frame of *NvTRPM2* was adapted to the human version. As a result, the induced frameshift as well as the position of the premature stop codon are not identical to the corresponding variant generated in *vivo* (Fig. 1, C). However, these small differences are not considered functionally relevant. We refer to this channel variant as NvTRPM2^{1008Stop}, indicating the slightly shifted position of the stop codon.

Surface expression of the NvTRPM2^{1008Stop} channel variant in HEK-293 cells

First, we analysed surface expression of the NvTRPM2^{1008Stop} channel in transiently transfected HEK-293 cells using a commercially available cell surface biotinylation assay. Transfected cells were exposed to biotinylation and subsequently the cell lysates were examined with SDS-PAGE gel electrophoresis and Western blot analysis. For effective detection in Western blot analysis, we used triple hemagglutinin (3xHA)-tagged variants both of wild-type NvTRPM2 (positive control) and NvTRPM2^{1008Stop} (ref. to Experimental Procedures). The anti-HA-tag antisera detected clear signals in the HA-tagged samples corresponding to the calculated mass of wild-type NvTRPM2-3xHA (175 kDA) and NvTRPM2^{1008Stop}-3xHA (115 kDA) **(Fig. 2, lanes 1, 2, 4, 5)**. Thus, the input control showed strong expression of wild-type NvTRPM2 as well as NvTRPM2^{1008Stop} channels, whereas no specific expression could be detected in mock transfected control cells **(Fig. 2, lanes 4 - 6)**. Likewise, in the biotinylated membrane fraction both wild-type NvTRPM2 and NvTRPM2^{1008Stop} mutant demonstrated comparable surface expression levels, whereas no signals could be detected in mock transfected control cells **(Fig. 2, lanes 1 - 3)**. Thus, despite its aberrant structure the surface expression of the truncated NvTRPM2^{1008Stop} protein was comparable to that of wild-type NvTRPM2. This result was not surprising because previous studies demonstrated regular surface expression of similarly truncated splice variants of HsTRPM2 (Zhang et al., 2003).

Channel function of the NvTRPM2^{1008Stop} channel variant in HEK-293 cells

For the functional characterization of the NvTRPM2^{1008Stop} channel variant in *vitro* we performed whole-cell patch clamp experiments of transiently transfected HEK-293 cells. As demonstrated in **Figure 3** (left panel) wild-type NvTRPM2 exhibited typical currents after stimulation with moderate concentrations of ADPR (0.15 mM) and Ca^{2+} (1µM) both applied through the pipette solution. Immediately after breaking into the cell at a holding potential of –60 mV strong inward currents developed, reaching maximum amplitudes within less than 5 s. Afterwards, a rapid current decline took place that reduced the current amplitude to less than 15 % within 30 s. Substitution of extracellular Na^{+} with the impermeable cation NMDG blocked the inward component of the current. In strong contrast, no such currents could be induced when HEK-293 cells transfected with NvTRPM2^{1008Stop} were stimulated with ADPR and Ca^{2+}. Even if a very high concentration (1.25 mM) of ADPR was applied, there was no significant current response detectable **(Fig. 3, right panel)**. Therefore, the

expression/function analysis of an almost identical channel variant in *vitro* strongly suggests that our NvTRPM2^{1016Stop} mutant represents a loss-of-function allele.

Validation of specific antisera to detect expression of NvTRPM2 in *vitro* and in *vivo*

Since no standard antisera were available as probes for NvTRPM2, three different antisera were produced. Most of the NvTRPM2 protein downstream of the pore region is constituted by the NUDT9H domain, and this part is absent in the NvTRPM2^{1016Stop} variant. For this reason, the application of C-terminus specific anti-TRPM2 antisera would be the method of choice. However, for NvTRPM2 this strategy is hampered by the fact that most likely the orthologue of the human NUDT9 enzyme is also expressed in *Nematostella*. The genome of *Nematostella* contains a predicted open reading frame of 281 amino acid residues that shows 45 % sequence identity with the human NUDT9 enzyme (350 amino acid residues; Kühn et al., 2017). Using an antiserum against human NUDT9, we detected bands of the expected size in Western blots from wild-type and NvTRPM2^{1016Stop} animals **(Suppl. Fig. 1)**. This finding indicates that antisera against the C-terminus of NvTRPM2 most probably would cross react with the endogenous NUDT9 orthologue of *Nematostella*.

We therefore selected epitopes in the N-terminal part of NvTRPM2 for generation of antisera, although these epitopes would be present in both control animals and in NvTRPM2$^{\mathbf{1016Stop}}$ mutants. While these antisera cannot be validated using NvTRPM2$^{\mathbf{1016Stop}}$ mutants for immunofluorescence, they could in principle be validated by Western blot of mutants and control animals. For this purpose we applied a special membrane fractionation protocol using differential centrifugation (Vriens et al., 2005). This method proved successful in our laboratory for the detection of diverse heterologously expressed ion channels (Winking et al., 2012). Unfortunately, all our attempts to detect NvTRPM2 by Western blot from wildtype or mutant animals failed (data not shown). Most probably, this was due to the fact that only limited cell material was available for Western blot analysis resulting in an inefficient preparation of cell membranes. In addition, it cannot be ruled out that the protocol by Vriens et al. (2005) did not work with our Nematostella preparations.

We next turned to the heterologous expression of NvTRPM2 in HEK-293 cells to test the specificity of our anti-NvTRPM2 antisera in comparison to the standard anti-HA antisera. As a result, especially antiserum "type N2" allows specific identification of both full-length wild-type NvTRPM2 and truncated NvTRPM2^{1016Stop} variant **(Suppl. Fig. 2).**

Therefore, our "type N2" antiserum represents a promising tool to investigate the general expression of NvTRPM2 in *Nematostella* in more detail.

Analysis of NvTRPM2 expression in *Nematostella* by immunofluorescence

Based on the data obtained from the preliminary experiments, we decided to examine the expression of wild-type NvTRPM2 in *Nematostella* by immunofluorescence and confocal microscopy. Therefore, we used different developmental stages of *Nematostella* that were stained for DNA (Hoechst) and NvTRPM2 (anti-NvTRPM2-antiserum "type N2"). As shown in **Figure 4** all analysed larval developmental stages were labelled by anti-NvTRPM2-antiserum. In the gastrula the expression of NvTRPM2 was identified in two distinct locations: First, in numerous single round-shaped cells that were distributed all over the animal **(Fig. 4, gastrula panel A and B, indicated by arrowheads)**. The number of these cells varied in the different focal planes of the animal. Second, in a layer surrounding the whole gastrula and most likely representing the plasma membrane of the outer cells (**Fig. 4, gastrula panel A and B)**. The same expression profile of NvTRPM2 was detected in planula larvae. In addition, we observed positive signals in elongated cellular regions of the pharynx **(Fig. 4, planula panel C, indicated by arrow)**. However, this could be unspecific staining of cnidocysts (the capsules of stinging cells), as has been observed with other immunofluorescence probes (Gahan and Rentzsch, unpublished observation). Similar potentially unspecific staining of cnidocysts was observed in juvenile polyps **(Fig. 4, juvenile polyp panel E and F, indicated by arrow)**. Moreover, in juvenile polyps the signals for expression of NvTRPM2 in individual roundish cells seem to be less condensed but instead more distributed over the animal. Here, the expression of NvTRPM2 in the plasma membrane is especially pronounced, showing signals in a focal plane of the cells of the animal's surface **(Fig. 4, juvenile polyp panel D)**. Altogether, these results indicate that the expression of NvTRPM2 is not limited to a specific larval developmental stage or distinct animal structures. Furthermore, NvTRPM2-specific signals could be detected in the plasma membrane which is in accordance with its function as ion channel.

Reproduction and development of the NvTRPM2 mutants of *Nematostella* under standard environmental conditions.

To obtain homozygous *NvTRPM2*^{1016Stop} animals, we crossed heterozygous *NvTRPM2*^{1016Stop} F_1 animals and identified homozygous *NvTRPM2*^{1016Stop} F_2 animals by PCR and DNA sequencing. We further in-crossed the homozygous F2s to obtain homozygous *NvTRPM2*^{1016Stop} F_3 animals that reached the adult stage. Thus, under our culture conditions, reproduction is not impaired in the heterozygous and homozygous *NvTRPM2*^{1016Stop} polyps. Likewise, the development from fertilized eggs to adult animals is not noticeably affected in *NvTRPM2*^{1016Stop} animals. The different developmental stages exhibited no visible difference

from wild-type animals, and we did not observe a delay in development **(Suppl. Fig. 3**). The fertilized eggs developed first into blastulae which then underwent gastrulation by invagination (Kraus and Technau, 2006; Magie et al., 2007). Afterwards, the animals elongated into a free swimming planula larvae with a tuft of long cilia at the aboral pole. The animals elongated further, and first tentacle buds arose. Finally, by elongation of body and tentacles the 4-tentacle-polyp stage was reached.

From then the growth beyond the 4-tentacle-polyp stage depended on nutritional status (Ikmi et al., 2020). Regular feeding of wildtype as well as *NvTRPM2*^{1016Stop} animals led to adult individuals that did not differ in their appearance.

In summary, neither reproduction nor the development of *Nematostella* from fertilized eggs to the adult stage was significantly impaired by the mutation of *NvTRPM2*.

Phenotypic characterization of the NvTRPM2 mutant animals under oxidative stress conditions.

In humans there is ample evidence for a central role of TRPM2 in oxidative stress-mediated apoptosis (e.g., Malko and Jiang, 2020). Accordingly, in transiently transfected HEK-293 cells the human TRPM2 channel can be readily activated by extracellular application of H_2O_2 (Hara et al., 2002; Wehage et al., 2002). For NvTRPM2, however, under the same experimental conditions the sensitivity to H_2O_2 strongly depends on the catalytic activity of the endogenous NUDT9H domain (Kühn et al., 2016, 2019). It is therefore possible that in *Nematostella* the NvTRPM2 channel is also involved in the responses to oxidative stress, but this process might be differently regulated, when compared to mammalian cells.

Intraspecific variations in the sensitivity to H_2O_2 of different populations of *Nematostella* were discovered in a previous study (Friedman et al., 2018), using concentrations of H_2O_2 between 0.00025 and 0.0005 % continuously applied throughout the experiments. In our study we decided to analyse the physiological role of NvTRPM2 in the response to oxidative stress in *vivo* by transient (5h) incubation of primary polyps (4-tentacle-polyps) to 0.00025 % H_2O_2. In our preliminary experiments this concentration, as well as the transient incubation, were found to induce tissue damage without killing most animals tested. Thus, our H_2O_2 treatment was effective but not lethal. For more details of the treatment with H_2O_2 as well as the procedures to categorize the resulting tissue damage see section “Experimental Procedures”. The treated animals of both genotypes were analysed for signs of tissue damage at selected times after transient exposure to H_2O_2. The applied time course of 1, 2, 3 and 15 days was used because *Nematostella* shows fast body regeneration after injury, i.e., in the analysed time

period we wanted to exclude significant attenuation of stress-induced lesions by regeneration effects.

Representative images demonstrating the effect of H_2O_2 treatment on wild-type and *NvTRPM2*^{1016Stop} 4-tentacle-polyps are depicted in **Figure 6**. In control animals both body column and tentacles were extended and the mesenteries were visible in the gastrovascular cavity with some distance to the tissue of the body column **(Fig. 5, panel A)**. After H_2O_2 treatment different degrees of tissue damage were observed in wildtype as well as *NvTRPM2*^{1016Stop} animals. Whereas some animals suffered minor damage, others were completely dissociated **(Fig. 5, panel C versus E and G)**. Most of the H_2O_2-treated animals showed pronounced body shrinking with mesenteries and gastrovascular cavity being invisible. Additionally, the length of the tentacles was strongly decreased. While some of the treated animals recovered to some extent over time, others deteriorated further and finally dissociated completely **(Fig. 5, panel E and G)**.

To get more insight into the induced tissue damage on a tissue level we performed confocal microscopy after staining tissues with phalloidin coupled to a fluorescent dye **(Fig. 5, right panels).** In this way, filamentous actin structures were made visible, which mainly belong to the muscle system of *Nematostella*. This muscle system consists of longitudinal retractor muscles in the tentacles, of longitudinal retractor muscles in the mesenteries (infoldings of the body column endoderm), and of longitudinal parietal muscles and circumferential ring muscle, both located in the body column (Jahnel et al. 2015). Therefore, we used the results of our phalloidin staining experiments to refine our observations of the living polyps.

The phalloidin staining of control and H_2O_2-treated animals revealed clear differences in the structure of actin fibres **(Fig. 5).** In control animals, longitudinal actin fibres of the body column were observed extending along the oral-aboral axis and the gastrovascular cavity was visible. The actin fibres within the tentacles were also visible near the oral opening **(Fig. 5, panel B)**. In contrast, H_2O_2-treated animals more often displayed small changes of actin fibres. The length of actin fibres was slightly reduced in the shrunken tentacles and the gastrovascular cavity **(Fig. 5, panel D)**. Moreover, some H_2O_2-treated animals also showed strongly truncated actin fibres within the shrunken tentacles or even the complete absence of actin fibres and tentacles. The originally elongated longitudinal actin fibres of the body column were contracted so that the gastrovascular cavity was constricted **(Fig. 5, panel F and H)**. In some of these animals the signals for actin fibres were no longer linear (an indication for elongated actin fibres), instead only punctual actin fibre signals could be detected **(Fig. 5, panel H)**. This observation points to a severe perturbation of the animal's muscular system.

Animals of both genotypes displayed the same spectrum of possible tissue damage, and all H_2O_2-treated animals were assigned to one of the two categories of "mild" or "severe" tissue damage. We compared the frequency of occurrence of the two categories of tissue damage between wildtype and *NvTRPM2*^{1016Stop} animals **(Fig. 6)**. In total 60 animals of each genotype were analysed, and 15 days after H_2O_2 treatment the portion of animals displaying a mild degree of H_2O_2-induced tissue damage was significantly increased in *NvTRPM2*^{1016Stop} (60 % of all analysed *NvTRPM2*^{1016Stop} animals), compared to wildtype (35 % of all analysed wild-type animals) animals **(Fig. 6, left panel)**. In contrast the number of animals displaying a severe degree of H_2O_2-induced tissue damage was significantly decreased in *NvTRPM2*^{1016Stop} (40 % of all analysed *NvTRPM2*^{1016Stop} animals), compared to wildtype (65 % of all analysed wild-type animals) animals **(Fig. 6, right panel)**. These data strongly suggest that in *Nematostella* the NvTRPM2 channel participates in the response to oxidative stress most likely by mediating tissue damage. Consequently, NvTRPM2 channels must be sensitive to H_2O_2 in *vivo* and on the basis of the divergent in *vitro* data (Kühn et al., 2015, 2016, 2019) need to be regulated in some way in *Nematostella*.

Phenotypic characterization of the *NvTRPM2* mutant animals under conditions of high temperatures.

Substantial fluctuations in water temperature are a hallmark of the natural habitat of *Nematostella*. Furthermore, it was demonstrated that for marine invertebrates higher water temperatures are intimately related with conditions of oxidative stress (Sheader et al., 1997; Durán et al., 2019).

The human TRPM2 orthologue was shown to be directly activated by temperatures which are in the range of our applied stress-test temperature (Tan and McNaughton, 2016; Song et al., 2016; Kashio and Tominaga, 2017). Therefore, we wanted to test whether mutation of *NvTRPM2* also affects high temperature-induced injury in *Nematostella*. For this purpose, we analysed the effects of high temperature (38.9°C) on the phenotype of wild-type and *NvTRPM2*^{1016Stop} animals using a similar design to the H_2O_2 exposure experiment. Intraspecific variations in temperature sensitivity of different populations of *Nematostella* have been described in the literature (Reitzel et al., 2013), with all developmental stages having critical temperatures within 1 °C (39.5 – 40.5°C). In preliminary experiments we found that incubation at 38.9°C for six hours was effective but not lethal and therefore we performed the experiments at this temperature. For more details of the exposure to high temperature as well as the procedures to categorize the resulting tissue damage see section

Experimental Procedures. In total 60 animals of each genotype, both wildtype and *NvTRPM2*^{1016Stop}, were analysed and the different degrees of tissue damage that were induced after high temperature stress corresponded to those observed after treatment with H_2O_2. Consequently, we used the same categories to estimate the effects on tissue damage.

Before starting the experiment, animals were in an extended state with phenotypical characteristics as described before. Likewise, the occurrence and specific distribution of high temperature-induced tissue damage were similar to those observed after exposure to oxidative stress. However, the relative effects of temperature stress on wildtype and *NvTRPM2*^{1016Stop} polyps turned out to be the opposite of those induced by oxidative stress. The experimental data revealed that 15 days after high-temperature treatment the number of animals displaying a mild degree of tissue damage was significantly decreased in *NvTRPM2*^{1016Stop} (27 % of all analysed *NvTRPM2*^{1016Stop} animals), if compared to wild-type (45 % of all analysed wild-type animals) animals **(Fig. 7, left panel)**. In contrast the portion of animals displaying a severe degree of H_2O_2-induced tissue damage was significantly increased in *NvTRPM2*^{1016Stop} (73 % of all analysed *NvTRPM2*^{1016Stop} animals), compared to wildtype (55 % of all analysed wild-type animals) animals **(Fig. 6, right panel).** Thus, it seems that NvTRPM2 does not mediate high temperature stress but protects sea anemones from harmful effects induced by this stressor.

Discussion

Our comparative analysis of the phenotypes of wildtype and *NvTRPM2*^{1016Stop} animals reveals that NvTRPM2 mediates tissue damage in *Nematostella* after exposure to oxidative stress. The observed injuries after temporary treatment with 0.00025 % H_2O_2 are significantly reduced in the *NvTRPM2*^{1016Stop} animals compared to wild-type animals. Using phalloidin staining we could show that in damaged tissues the actin fibres of the cytoskeleton were strongly impaired. This disintegration of intracellular structures might point to apoptosis, which would be in line with the data obtained from the human TRPM2 orthologue (e.g., Yamamoto et al. 2008; Uchida et al. 2014; Miller et al. 2016). However, while in human cells TRPM2 can be readily stimulated with H_2O_2 both in *vitro* and in *vivo* (Perraud et al. 2005; Fonfria et al. 2005; Buelow et al. 2008; Hara et al. 2002; Hecquet et al. 2014), this is not the case for NvTRPM2 during heterologous expression in HEK-293 cells (Kühn et al., 2015, 2016, 2019). Most probably this is caused by the NUDT9H domain of NvTRPM2, since suppression of its ADPRase function in *vitro* directly leads to the sensitization of the channel to H_2O_2 (Kühn et al., 2016, 2017, 2019).

Oxidative stress in the form of reactive oxygen species can be generated both inside the cell, e.g., as by-products of an (inadequate) respiratory chain, and through external environmental influences on the organism. The applied concentrations of 0.00025 % (82 µM) H_2O_2 in our experiments is within the range of concentrations used in another study which examined intraspecific variations in oxidative stress tolerance of adult *Nematostella* (Friedman et al., 2018). In the same study it was shown that continuous incubation with twice the concentration (0.0005 %) of H_2O_2 already leads to a drastic increase in the mortality rate of adult animals, which reaches almost 100 % with a further increase in concentration (Friedman et al., 2018). In contrast, in our comparative stress test analysis we used primary polyps (4-tentacle-polyps) instead of adult animals of *Nematostella*, and both the applied concentration and the exposure time of H_2O_2 treatment was adjusted to a sub-lethal range. Remarkably, for the extracellular stimulation of TRPM2 in transfected HEK-293 cells bolus concentrations of H_2O_2 in the high micromolar to millimolar range are necessary (Bari et al., 2010; Zou et al., 2013). This usually induces strong channel activation and subsequently cellular apoptosis within a few minutes (e.g., Wehage et al., 2002; Sun et al., 2012). It is very likely that only a fraction of this extracellular bolus addition will be effective inside the cell because various cytosolic enzymes rapidly decompose H_2O_2. For the same reason, the effective concentrations of H_2O_2 in *vivo* are difficult to estimate, especially since extracellular bolus addition of H_2O_2 does not lead to a uniform spatiotemporal distribution of H_2O_2 throughout the cell (Lim et al., 2016).

According to a previous study our applied concentration of H_2O_2 is in the upper range of levels recorded in aquatic environments comparable to the natural habitat of *Nematostella* (Abele-Oeschger et al., 1997).

Notably, oxidative stress stimulates TRPM2 in an indirect manner and channel activation represents only one of several steps in the pathway of cellular apoptosis (Perraud et al., 2005; Pascal and Ellenberger, 2015). In the case of *Nematostella* there is experimental evidence that the sensitivity to H_2O_2 could be regulated by the catalytic activity of the endogenous NUDT9H domain of NvTRPM2 (Kühn et al., 2016, 2019). In addition, our current study revealed significant expression of an orthologue of the human ADPRase NUDT9 in *Nematostella*. Thus, the oxidative stress-induced accumulation of cytosolic ADPR as crucial trigger of NvTRPM2 activation might be suppressed by two independent ADPRases. This scenario could result in an increased threshold for the H_2O_2-dependent activation of NvTRPM2 in *vivo* and may be subject to a special, currently unknown regulatory mechanism.

In light of our finding that NvTRPM2 and NvNUDT9 are expressed in *Nematostella*, it can be assumed that also in this species ADP-ribose plays an important role as an intracellular

signalling molecule. Further studies will be necessary to compare the physiological relevance of ADPR in *Nematostella* and other sea anemones with its pivotal role in mammals. The development of NUDT9-based ADPR-FRET sensors would represent a promising tool that may help with the analysis of cellular ADPR signalling processes in the future (Gattkowski et al., 2021).

Acute environmental stress e.g., induced by shifts of temperature, pH and osmolarity can interfere with the cellular redox balance leading to the increased production of reactive oxygen species (Tomanek, 2015). On the other hand, the organism has the ability to adjust the production of antioxidant enzymes in response to acute fluctuations of local temperature. This is not only the case for marine invertebrates (Handy et al., 2009) but generally occurs in all eukaryotic cells (Durán et al., 2019). In addition, the mammalian TRPM2 channel has been described as sensitive both to oxidative stress and higher temperatures whereby oxidative stress sensitizes TRPM2 to heat (Kashio et al., 2012; Kashio and Tominaga, 2017).

Therefore, regarding the effects of high temperature on the phenotype of wildtype and *NvTRPM2*^{1016Stop} *Nematostella*, similar results as obtained by oxidative stress treatment were expected. Instead, our experimental findings revealed that NvTRPM2 attenuates tissue damage induced by high temperature treatment, and thus exerts a protective function in *Nematostella*. At first glance, this result seems to be difficult to reconcile with previous findings, in particular the stimulating effects of H_2O_2 and higher temperatures on mammalian TRPM2 channels. However, it must be taken into account that the activation mechanism of NvTRPM2 in *Nematostella* is remarkably different from the mammalian orthologues. As mentioned above, the sensitivity of NvTRPM2 to H_2O_2 strongly depends on the enzymatic activity of the endogenous NUDT9H domain which is catalytically inactive in HsTRPM2 (Kühn et al., 2016, 2019; Iordanov et al., 2016, 2019). Furthermore, the temperature sensitivity of NvTRPM2 has not yet been investigated, and therefore it cannot be excluded that high temperatures do not directly affect NvTRPM2. On the other hand, it is conceivable that higher temperatures to a certain degree not only stimulate antioxidant enzymes (Durán et al., 2019) but also ADPRases such as NUDT9 or the NUDT9H domain of NvTRPM2, leading to the degradation of the principal channel agonist ADPR. As a result, higher temperatures would attenuate rather than stimulate channel function of NvTRPM2. Nevertheless, all these considerations cannot explain our experimental findings, where in *Nematostella* loss of NvTRPM2 function aggravates tissue damage after exposure to high temperature.

Possibly, in *Nematostella* NvTRPM2 plays an entirely different physiological role in response to higher temperatures. Besides its well-established function as a mediator of oxidative stress-

induced apoptosis in mammals, there is also experimental evidence from TRPM2 knockout mice that TRPM2 can protect cardiac myocytes from ischemic injury by preventing mitochondrial dysfunction and increased ROS levels (Miller et al., 2014). In further studies genetic deletion of TRPM2 in mice was also shown to be neuroprotective in a developmental model of hypoxic-ischemic brain damage (Huang et al., 2017) or to reduce susceptibility to pneumoseptic infection by *Klebsiella pneumonia* corresponding with decreased bacterial burden and attenuated tissue pathology (Sharma et al., 2017). All these physiological processes are linked to specific regulation mechanisms which do not necessarily run via the classic ADPR pathway. However, a connection between the described protective role of TRPM2, and functional effects of higher temperature have not yet been investigated. At least in the case of infectious processes and the corresponding immune responses, a critical role of elevated temperatures in context with human TRPM2 is plausible (e.g. Knowles et al., 2013; Tan & McNaughton, 2018). However, the underlying mechanisms are not yet fully understood. Whether such processes in a rudimentary form also occur in marine invertebrates such as Nematostella is of course completely open.

In conclusion our experimental findings deliver first insights into the physiological role of TRPM2 in a basal metazoan and may open the door for detailed molecular studies on the stress-response of *Nematostella*. Further efforts are needed to examine thermoregulation of NvTRPM2 and to pinpoint the physiological role of ADPR in sea anemones. In this context, *Nematostella* could represent a valuable model system to characterize the physiological spectrum of TRPM2 function.

Acknowledgements

We thank Marina Wolf for expert technical assistance.

Funding

The study was supported by the Deutsche Forschungsgemeinschaft (DFG, Grant KU 2271/4-3 to FJPK).

Author contributions

FJPK and FR conceived the study. WE and JMG generated the TRPM2 loss of function mutation in Nematostella. WE performed cultivation of Nematostella, stress test analyses, biotinylation assays, confocal microscopy, Phalloidin stainings and Western-blot analyses. FJPK generated the loss of function variant of nvTRPM2 for in vitro analysis. WE and FJPK performed whole-cell patch-clamp experiments of HEK-293 cells. WE and FJPK conducted data analysis and prepared figures. FJPK and WE wrote the manuscript with input from all authors.

Competing interests: The authors declare no competing interests.

References

Abele-Oeschger, D., H. Tüg, and R. Röttgers, Dynamics of UV-driven hydrogen peroxide formation on an intertidal sandflat. American Society of Limnology and Oceanography, 1997. 12(6): p. 1406 - 1415.

Bari, MR. et al., H2O2-induced Ca2+ influx and its inhibition by N-(p-amylcinnamoyl) anthranilic acid in the beta-cells: involvement of TRPM2 channels. J Cell Mol Med., 2009. 13(9B):3260-7.

Buelow, B., Y. Song, and A.M. Scharenberg, The Poly(ADP-ribose) polymerase PARP-1 is required for oxidative stress-induced TRPM2 activation in lymphocytes. J Biol Chem, 2008. 283(36): p. 24571-83.

Darling, J.A., et al., Rising starlet: the starlet sea anemone, Nematostella vectensis. Bioessays, 2005. **27**(2): p. 211-21.

Dias, M., et al., Long-term exposure to increasing temperatures on scleractinian coral fragments reveals oxidative stress. Marine Environmental Research, 2019. 150(104758).

Downs, C.A., et al., Oxidative stress and seasonal coral bleeching. Free Radic Biol Med., 2002. 33(4): p. 533 – 43.

Elran, R., et al., Early and late response of Nematostella vectensis transcriptome to heavy metals. Mol Ecol, 2014. **23**(19): p. 4722-36.

Fonfria, E., et al., TRPM2 channel opening in response to oxidative stress is dependent on activation of poly(ADP-ribose) polymerase. Br J Pharmacol, 2004. 143(1): p. 186-92.

Fonfria, E., et al., Amyloid beta-peptide(1-42) and hydrogen peroxide-induced toxicity are mediated by TRPM2 in rat primary striatal cultures. J Neurochem, 2005. 95(3): p. 715-23.

Friedman, L.E., T.D. Gilmore, and J.R. Finnerty, Intraspecific variation in oxidative stress tolerance in a model cnidarian: Differences in peroxide sensitivity between and within populations of Nematostella vectensis. PLoS One, 2018. 13(1): p. e0188265.

Gattkowski, E. et al., Analysis of ligand-binding and resulting conformational changes in pyrophosphatase NUDT9. FEBS J., 2021.

González Durán, E., et al., Effects of Temperature and pH on the Oxidative Stress of Benthic Marine Invertebrates. Biology Bulletin, 2019. 45(6): p. 610-616.

Handy, D. et al., Glutathione peroxidase-1 regulates mitochondrial function to modulate redox-dependent cellular response, J. Biol. Chem., 2009. vol. 284, no. 18, pp. 11913–11921.

Hara, Y., et al., LTRPC2 Ca2+-Permaeble Channel Activated by Changes in Redox Status Confers Susceptibility to Cell Death. Molecular Cell, 2002. 9: p. 163-173.

Harter, V.L. and R.A. Matthews, Acute and chronic toxicity test methods for Nematostella vectensis Stephenson. Bull Environ Contam Toxicol, 2005. 74(5): p. 830-6.

Hecquet, C.M., et al., Cooperative interaction of trp melastatin channel transient receptor potential (TRPM2) with its splice variant TRPM2 short variant is essential for endothelial cell apoptosis. Circ Res, 2014. 114(3): p. 469-79.

Huang, S., et al. Transient receptor potential melastatin 2 channels (TRPM2) mediate neonatal hypoxic-ischemic brain injury in mice. Exp. Neurol. (2017). 296, 32–40.

Huang, Y., et al., Architecture of the TRPM2 channel and its activation mechanism by ADP-ribose and calcium. Nature, 2018.

Huang, Y., et al., Ligand recognition and gating mechanism through three ligand-binding sites of human TRPM2 channel. eLife, 2019.

Ikmi, A., et al., TALEN and CRISPR/Cas9-mediated genome editing in the early-branching metazoan Nematostella vectensis. Nat Commun, 2014. **5**: p. 5486.

Ikmi, A., et al., Feeding-dependent tentacle development in the sea anemone Nematostella vectensis. Nat Commun, 2020. **11**(1): p. 4399.

Iordanov, I., et al., The proposed channel-enzyme transient receptor potential melastatin 2 does not possess ADP ribose hydrolase activity. Elife, 2016. 5.

Iordanov, I., et al., Enzyme activity and selectivity filter stability of ancient TRPM2 channels were simultaneously lost in early vertebrates. Elife, 2019. 8.

Jahnel, S., M. Walzl, and U. Technau, Development and epithelial organisation of muscle cells in the sea anemone Nematostella vectensis. Frontiers in Zoology, 2014. 11(44).

Kashio, M., et al., Redox signal-mediated sensitization of transient receptor potential melastatin 2 (TRPM2) to temperature affects macrophage functions. Proc Natl Acad Sci U S A, 2012. 109(17): p. 6745-50.

Kashio, M. and M. Tominaga, The TRPM2 channel: A thermo-sensitive metabolic sensor. Channels (Austin), 2017. 11(5): p. 426-433.

Knowles, H., Y. Li, and A.-L. Perraud, The TRPM2 ion channel, an oxidative stress and metabolic sensor regulating innate immunity and inflammation. Immunologic Research, 2013. **55**(1-3): p. 241-248.

Kraus, Y. and U. Technau, Gastrulation in the sea anemone Nematostella vectensis occurs by invagination and immigration: an ultrastructural study. Dev Genes Evol, 2006. **216**(3): p. 119-32.

Kraus, Y., et al., Pre-bilaterian origin of the blastoporal axial organizer. Nat Commun, 2016. **7**: p. 11694.

Kuhn, F.J., C. Kuhn, and A. Luckhoff, Functional characterisation of a TRPM2 orthologue from the sea anemone Nematostella vectensis in human cells. Sci Rep, 2015. 5: p. 8032.

Kuhn, F.J., et al., ADP-Ribose Activates the TRPM2 Channel from the Sea Anemone Nematostella vectensis Independently of the NUDT9H Domain. PLoS One, 2016. 11(6): p. e0158060.

Kuhn, F., C. Kuhn, and A. Luckhoff, Different Principles of ADP-Ribose-Mediated Activation and Opposite Roles of the NUDT9 Homology Domain in the TRPM2 Orthologs of Man and Sea Anemone. Front Physiol, 2017. 8: p. 879.

Kuhn, F.J.P., et al., Functional importance of NUDT9H domain and N-terminal ADPR-binding pocket in two species variants of vertebrate TRPM2 channels. Sci Rep, 2019. 9(1): p. 19224.

Kuhn, F.J.P., Structure-Function Relationship of TRPM2: Recent Advances, Contradictions, and Open Questions. Int J Mol Sci, 2020. 21(18).

Layden, M.J., F. Rentzsch, and E. Rottinger, The rise of the starlet sea anemone Nematostella vectensis as a model system to investigate development and regeneration. Wiley Interdiscip Rev Dev Biol, 2016. **5**(4): p. 408-28.

Lim JB, Langford TF, Huang BK, Deen WM, Sikes HD. A reaction-diffusion model of cytosolic hydrogen peroxide. Free Radic Biol Med. 2016 Jan;90:85-90. doi: 10.1016/j.freeradbiomed.2015.11.005. Epub 2015 Nov 10. PMID: 26561774.

Magie, C.R., M. Daly, and M.Q. Martindale, Gastrulation in the cnidarian Nematostella vectensis occurs via invagination not ingression. Dev Biol, 2007. **305**(2): p. 483-97.

Malko, P. and L.H. Jiang, TRPM2 channel-mediated cell death: An important mechanism linking oxidative stress-inducing pathological factors to associated pathological conditions. Redox Biol, 2020. 37: p. 101755.

Miller, D.J., et al., The innate immune repertoire in cnidaria--ancestral complexity and stochastic gene loss. Genome Biol., 2007. 8(4): R59.

Miller, B.A., et al., TRPM2 channels protect against cardiac ischemia-reperfusion injury: role of mitochondria. J Biol Chem, 2014. 289(11): p. 7615-29.

Miller, B.A. and J.Y. Cheung, TRPM2 protects against tissue damage following oxidative stress and ischaemia-reperfusion. J Physiol, 2016. 594(15): p. 4181-91.

Pascal, J.M. and T. Ellenberger, The rise and fall of poly(ADP-ribose): An enzymatic perspective. DNA Repair (Amst), 2015. 32: p. 10-16.

Perraud, A.L., et al., ADP-ribose gating of the calcium-permeable LTRPC2 channel revealed by Nudix motif homology. Nature, 2001. 411.
Perraud, A.L., et al., NUDT9, a member of the Nudix hydrolase family, is an evolutionarily conserved mitochondrial ADP-ribose pyrophosphatase. J Biol Chem, 2003. 278(3): p. 1794-801.

Perraud, A.L., et al., Accumulation of free ADP-ribose from mitochondria mediates oxidative stress-induced gating of TRPM2 cation channels. J Biol Chem, 2005. 280(7): p. 6138-48.

Putnam, N., et al., Sea Anemone Genome Reveals Ancestral Eumetazoan Gene Repertoire and Genomic Organization. Science, 2007. 317(5834): p. 86 - 94.

Reitzel, A.M., et al., Genomic Survey of Candidate Stress-Response Genes in the Estuarine Anemone Nematostella vectensis. Biol. Bull., 2008. **214**: p. 233 - 254.

Reitzel, A., et al., Physiological and developmental responses to temperature by the sea anemone Nematostella vectensis. Marine Ecology Progress Series, 2013. 484: p. 115 - 130.

Rivera, H.E., et al., Plasticity in parental effects confers rapid larval thermal tolerance in the estuarine anemone Nematostella vectensis. J Exp Biol, 2021. **224**(Pt 5).

Sharma, J., et al., Protective function of Calcium permeable cation channel TRPM2 during pneumoseptic Klebsiella pneumoniae infection. The Journal of Immunology, 2017. 198(1).

Sheader, M., M. Suwailem, and G. Rowe, The anemone, Nematostella vectensis, in Britain: Considerations for conservation management. Aquatic Conservation: Marine and Freshwater Ecosystems, 1997. 7: p. 13-25.

Song, K., et al., The TRPM2 channel is a hypothalamic heat sensor that limits fever and can drive hypothermia. Science, 2016. 353(6306): p. 1393-1398.

Stefanik, D.J., L.E. Friedman, and J.R. Finnerty, Collecting, rearing, spawning and inducing regeneration of the starlet sea anemone, Nematostella vectensis. Nat Protoc, 2013. 8(5): p. 916-23.

Sullivan, J.C., et al., StellaBase: the Nematostella vectensis Genomics Database. Nucleic Acids Res, 2006. 34(Database issue): p. D495-9.

Sun, L. et al., Role of TRPM2 in H_2O_2-induced cell apoptosis in endothelial cells. PLoS One., 2012. 7(8): e43186.

Tan, C.H. and P.A. McNaughton, The TRPM2 ion channel is required for sensitivity to warmth. Nature, 2016. 536(7617): p. 460-3.

Tan, C.H. and P.A. McNaughton, TRPM2 and warmth sensation. Pflugers Arch., 2018. 470(5): p. 787 – 798.

Tarrant, A.M., et al., Activation of the cnidarian oxidative stress response by ultraviolet radiation, polycyclic aromatic hydrocarbons and crude oil. J Exp Biol, 2014. **217**(Pt 9): p. 1444-53.

Technau, U., et al., Maintenance of ancestral complexity and non-metazoan genes in two basal cnidarians. Genome Analysis, 2005. 21(12): p. 633 - 639.

Tomanek, L. Proteomic responses to environmentally induced oxidative stress. J Exp Biol., 2015. 218(Pt 12):1867-79.

Uchida, K., et al., Lack of TRPM2 impaired insulin secretion and glucose metabolisms in mice. Diabetes, 2011. **60**(1): p. 119-26.

Uhlinger, C.H.a.K.R., The Culture, Sexual and Asexual Reproduction, and Growth of the Sea Anemone Nematostella vectensis. Biol. Bull., 1992. 182: p. 169-176.

Vriens, J., et al., Modulation of the Ca^{2+} permeable cation channel TRPV4 by cytochrome P450 epoxygenases in vascular endothelium. Circ Res., 2005. 97(9): p. 908 – 15.

Wehage, E., et al., Activation of the cation channel long transient receptor potential channel 2 (LTRPC2) by hydrogen peroxide. A splice variant reveals a mode of activation independent of ADP-ribose. J Biol Chem, 2002. 277(26): p. 23150-6.

Winking, M., et al., Importance of a Conserved Sequence Motif in Transmembrane Segment S3 for the Gating of Human TRPM8 and TRPM2. PLoS One, 2012. 7(11): e49877.

Yamamoto, S., et al., TRPM2-mediated Ca2+influx induces chemokine production in monocytes that aggravates inflammatory neutrophil infiltration. Nat Med, 2008. **14**(7): p. 738-47.

Zhang, W., et al., A novel TRPM2 isoform inhibits calcium influx and susceptibility to cell death. J Biol Chem, 2003. 278(18): p. 16222-9.

Zou, J. et al., A differential role of macrophage TRPM2 channels in Ca^{2+} signaling and cell death in early responses to H_2 O_2 . Am J Physiol Cell Physiol., 2013. 1;305(1): C61-9.

Figures

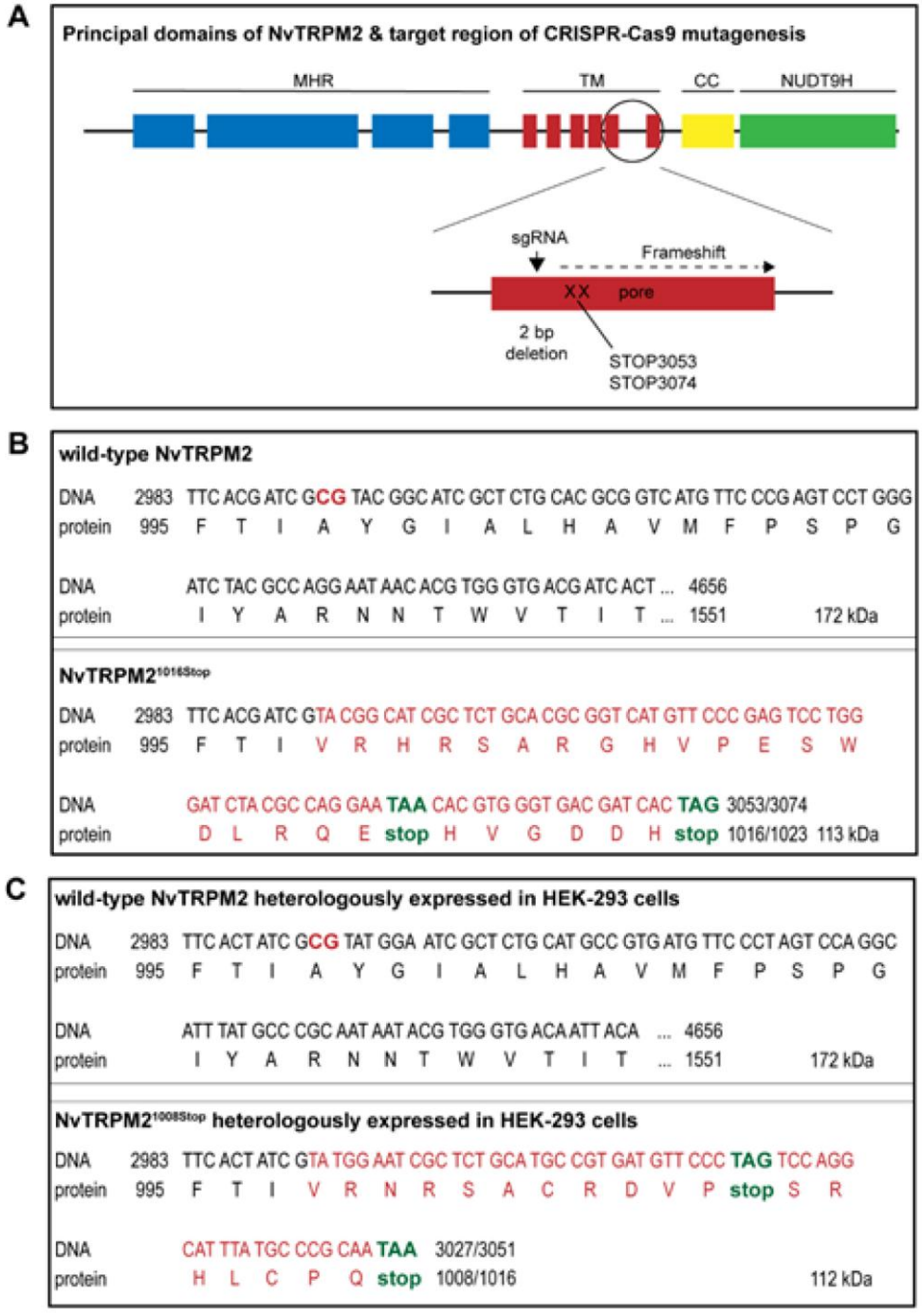

Figure 1: Primary domain structure of full length NvTRPM2 and sequence manipulations required for the generation of *NvTRPM2*^{1016Stop} in *vivo* as well as *NvTRPM2*^{1008Stop} in *vitro*. A The principal domains are TRPM homology region (MHR) transmembrane domains (TM) coiled-coil domain (CC) and NUDT9H. A two base pair deletion was introduced within the pore region (circled) by CRISPR-Cas9 mutagenesis. The resulting downstream (-2 bp) frameshift generates two premature stop codons (indicated by "X"). **B and C** Corresponding DNA- and amino acid sequences of the target pore region of *NvTRPM2* with modifications (given in red) for expression either in *vivo* (**B**) or in *vitro* (**C**). Relative positions are given at the beginning and at the end of the sequences. The calculated mass (kDa) of full-length wild-type channel and truncated channel variants are indicated.

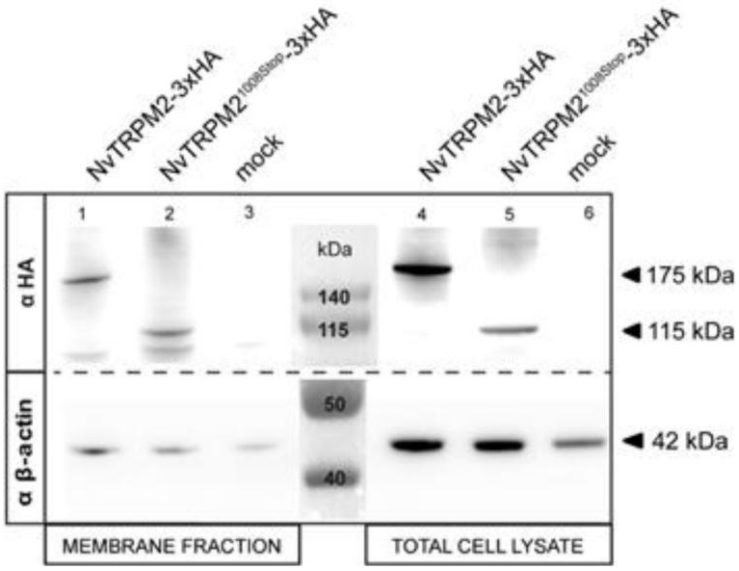

Figure 2: Cell surface expression of wild-type NvTRPM2 and NvTRPM2^{1008Stop} mutant in HEK-293 cells. Standard cell surface biotinylation assay was performed with the corresponding 3x-HA tagged channel variants heterologously expressed in HEK-293 cells. Biotinylated cell lysates were incubated with NeutrAvidin beads and afterwards eluted with SDS-sample buffer. Eluates and the corresponding total cell lysates (as indicated) were subjected to reducing SDS-PAGE gel electrophoresis and Western blot analysis. Mock-transfected cells were used as negative control. The Western blot membrane was cut between 50 and 65 kDA (indicated by dotted line) and incubated with commercially available anti-HA and anti-β-actin antibodies, respectively. Because of different staining intensities, variable exposure times were applied for the identification of HA and β-actin signals. Three independent experiments gave similar results.

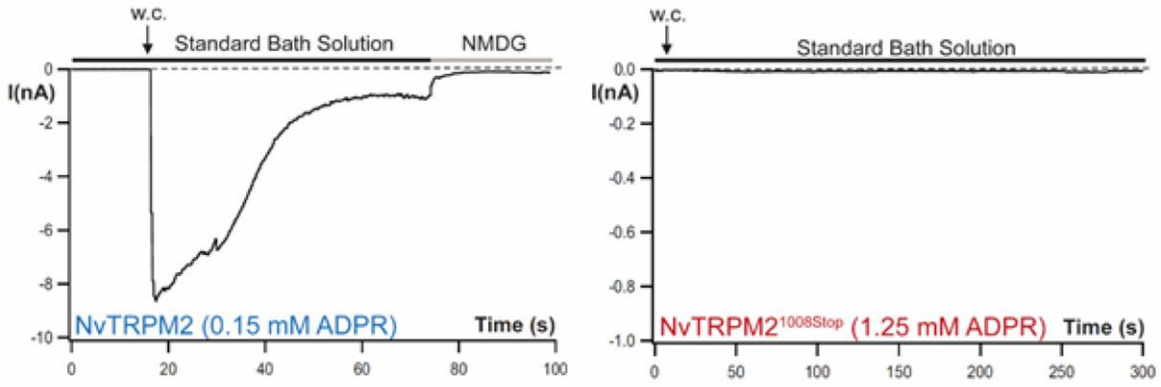

Figure 3: Whole-cell patch clamp analysis of wild-type NvTRPM2 and NvTRPM2^{1008Stop} channel variant heterologously expressed in HEK-293 cells. Transiently transfected cells were stimulated with ADPR (concentrations indicated) and Ca^{2+} (1 µM) applied through the patch pipette. Left panel: After establishing whole-cell configuration (″w.c.″) wild-type NvTRPM2 shows the typical current kinetics with very fast current increase followed by a spontaneous current decline. Substitution of extracellular Na^{+} with the impermeable cation NMDG blocked the inward currents. Right panel: No currents could be evoked in cells transfected with the NvTRPM2^{1008Stop} variant, even if a very high concentration (as indicated) of ADPR was applied. Six independent experiments gave similar results.

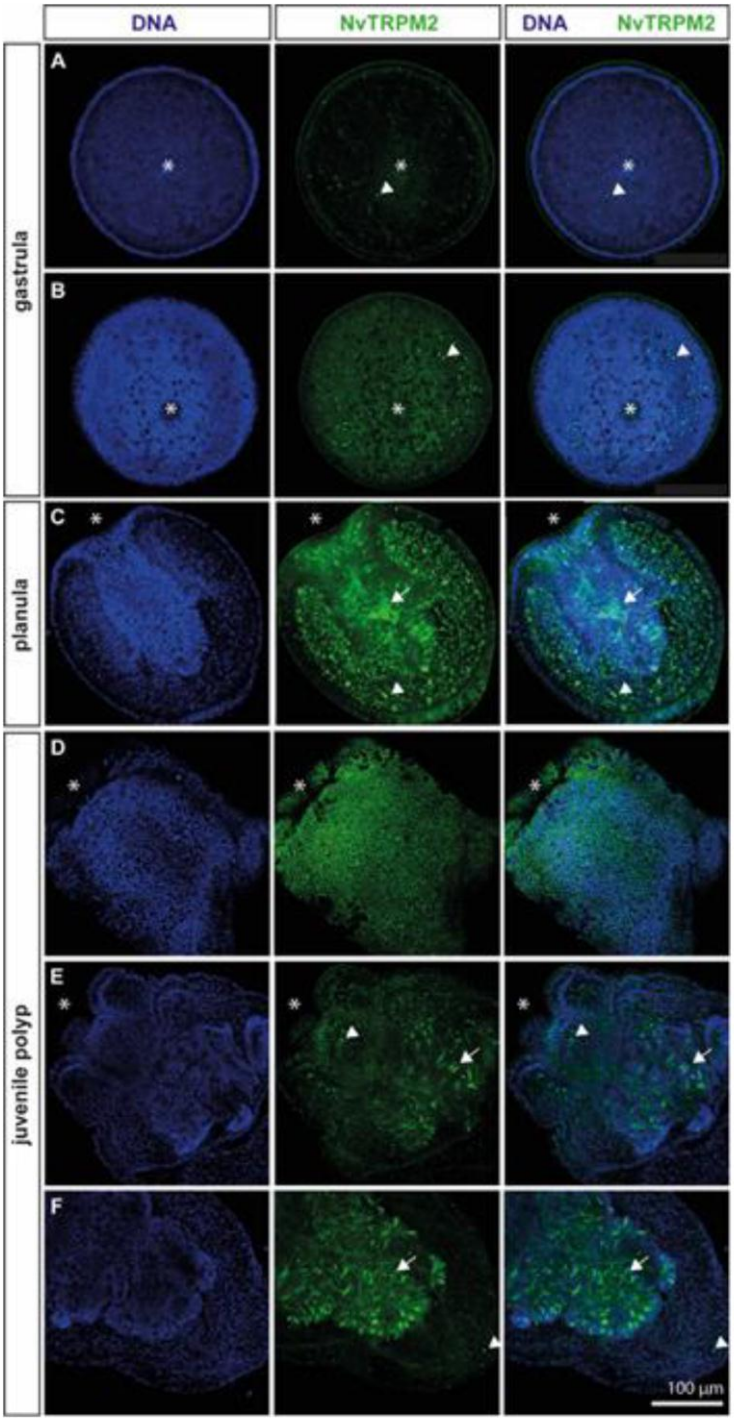

Figure 4: Representative immunofluorescence images showing expression of wild-type NvTRPM2 in distinct developmental stages of *Nematostella*. Different developmental stages of *Nematostella* (as indicated) were stained for DNA with Hoechst and probed with our specific anti-NvTRPM2 antiserum targeting an N-terminal epitope of NvTRPM2. The blastopore (site of future mouth) is marked by an asterisk. For the gastrula stage, two different focal planes of the same animal are shown (panels A and B). For the juvenile polyp stage, the panels D and E represent two different focal planes of different animals and panels E and F represent different areas of the same animal at the same focal plane. In all developmental stages tested, a distinct expression pattern of NvTRPM2 was detected. This includes single cells distributed all over the organisms (indicated with arrowheads) as well as the plasma membrane (gastrula, planula and juvenile polyp, panels A – D). Positive signals were also detected in cnidocysts (indicated by arrows) but most likely were unspecific (Gahan and

Rentzsch, unpublished observation). 10 experiments with 15 individual animals in each experiment gave similar results. Images were taken with a confocal microscope at 40x resolution and show the different channels for DNA and NvTRPM2 signals and the merge of both channels. For better visibility the brightness of the images was adjusted to +40 %. The scale bar represents 100 µm and can be applied to all images.

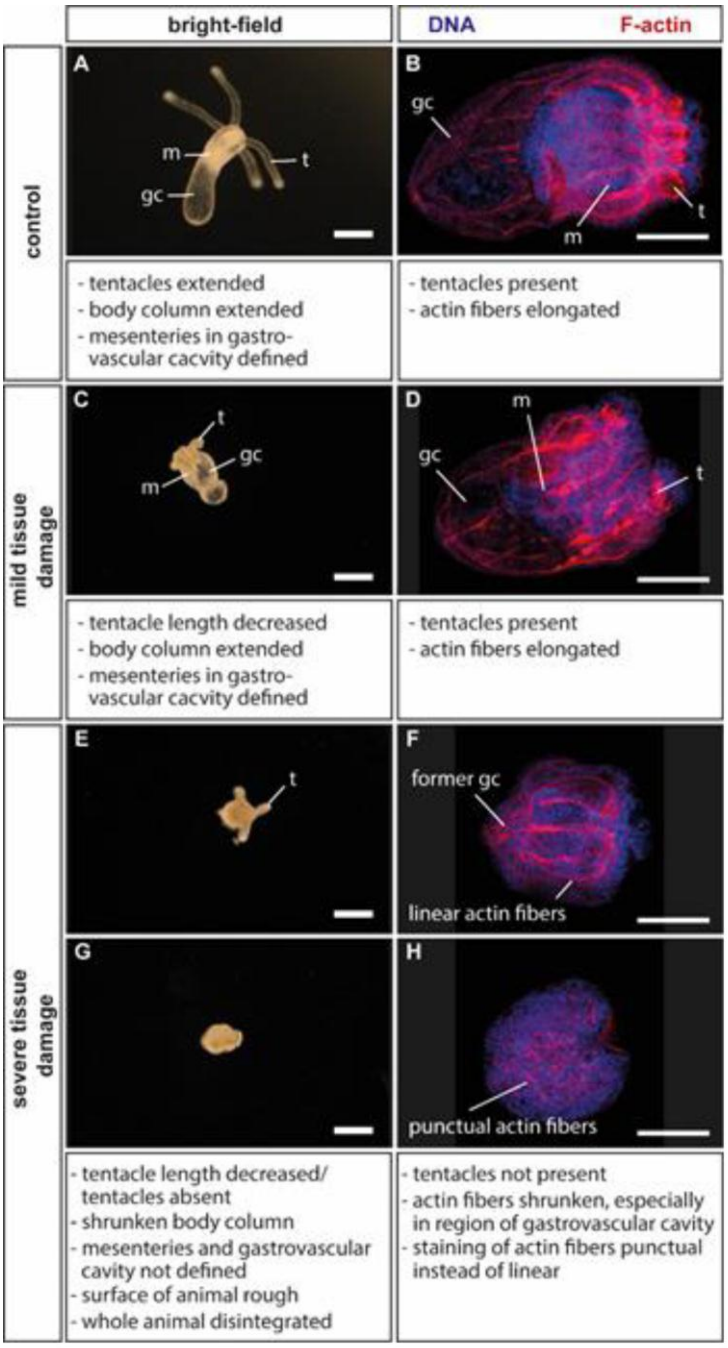

Figure 5: Classification of the degree of H_2O_2-induced tissue damage in 4-tentacle-polyps of *Nematostella*. Wild-type and *NvTRPM2*^{1016Stop} animals were transiently incubated for five hours with 0.00025 % H_2O_2. Bright-field microscopy images of the animals were taken before and 1, 2, 3 and 15 days after H_2O_2 treatment (left panels). Actin fibres were stained with phalloidin coupled to fluorescent dye Alexa 555 to analyse the effect of H_2O_2 treatment on the muscle system (actin fibres) of the animals (right panels). The categories of different degrees of tissue damage are indicated and treated animals were classified to the categories "mild" or "severe". Animals with mild tissue damage looked similar to the untreated control animals. In corresponding bright-field images, tentacles are present, mesenteries visible within the gastrovascular cavity and the body column is elongated (panel A and C). Phalloidin staining revealed staining of tentacle muscles and linear actin fibres that extent along the oral – aboral body axis (panel B and D). Animals that displayed severe tissue damage have very short or absent tentacles and a shrunken body column. The mesenteries are not visible within the gastrovascular cavity and some animals are completely disintegrated (panel E and G). Phalloidin staining revealed shrunken actin fibres, especially in the region of the former gastrovascular cavity and

less or no staining of tentacle muscles (panel F and H). Some animals show no linear but only punctual actin fibre staining, indicating a process of disintegration of inner muscle structures (panel H). 5 experiments with 15 individual animals in each experiment gave similar results. Important animal tissue structures are indicated: tentacles: t, mesenteries: m, gastrovascular cavity: gc. The scale bars represent 100 µm.

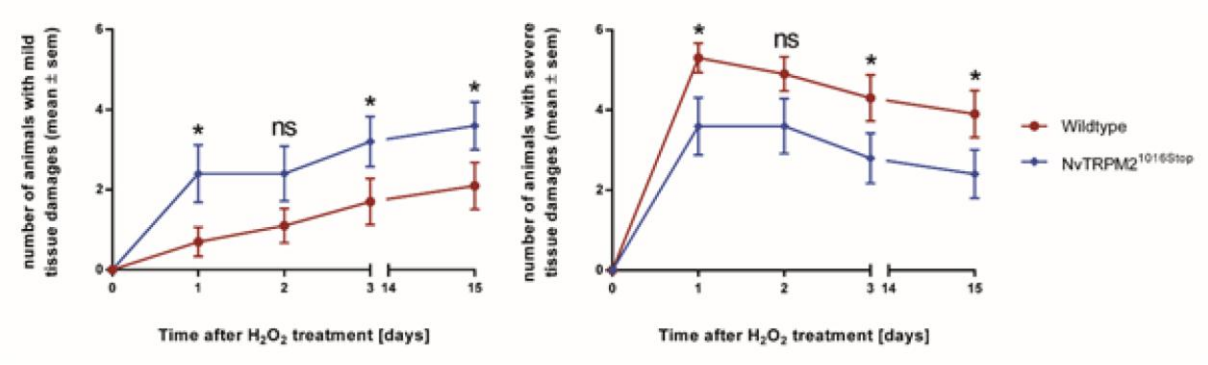

Figure 6: Effect of H_2O_2-induced tissue damage on 4-tentacle-polyps of wild-type and *NvTRPM2*^{1016Stop} animals. 4-tentacle-polyps were transiently incubated in NM supplemented with 0.00025 % H_2O_2 for five hours at standard culture conditions (18°C in the dark). Bright-field images were taken, and the degree of tissue damage was scored before treatment and 1, 2, 3 and 15 days after exposure to H_2O_2. For each experiment 6 wild-type and 6 *NvTRPM2*^{1016Stop} animals were analysed, and this experimental setting was repeated 10 times, so in total 60 animals of each genotype were analysed. The number of animals with mild (left panel) or severe (right panel) degree of tissue damage was significantly different between *NvTRPM2*^{1016Stop} and wild-type animals. Averaged values with SEM are shown, statistical analysis was performed with a 2-way ANOVA (n = 10, significant difference between genotypes p = 0.0005 and time after treatment < 0.0001) and Fisher's LSD post-hoc test (p-values < 0.005 *, ns = not significant).

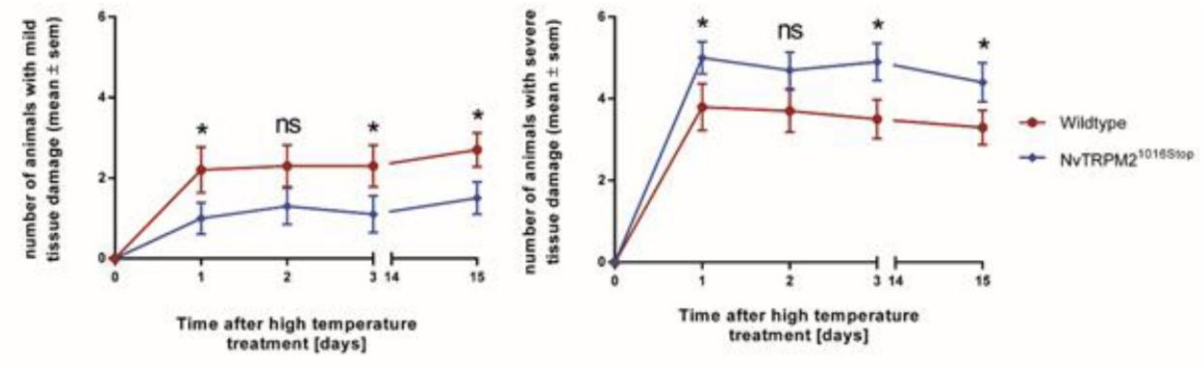

Figure 7: Effect of high temperature-induced tissue damage on 4-tentacle-polyps of wild-type and *NvTRPM2*^{1016Stop} animals. 4-tentacle-polyps were incubated in NM at 38.9°C for six hours using a PCR machine and afterwards returned to standard culture conditions (18°C in the dark). Bright-field images were taken, and the degree of tissue damage was scored before treatment and 1, 2, 3 and 15 days after high temperature treatment, respectively. For each experiment 6 wild-type and 6 *NvTRPM2*^{1016Stop} animals were analysed, and this experimental setting was repeated 10 times, so in total 60 animals of both genotypes were analysed. The number of animals with mild (left panel) or severe (right panel) degree of tissue damage was significantly different between *NvTRPM2*^{1016Stop} and wild-type animals. Averaged values with SEM are shown, statistical analysis was performed with a 2-way ANOVA (n = 10, significant difference between genotypes $p = 0.0008$ and time after treatment < 0.0001) and Fisher's LSD post-hoc test (p-values < 0.005 *, ns = not significant).

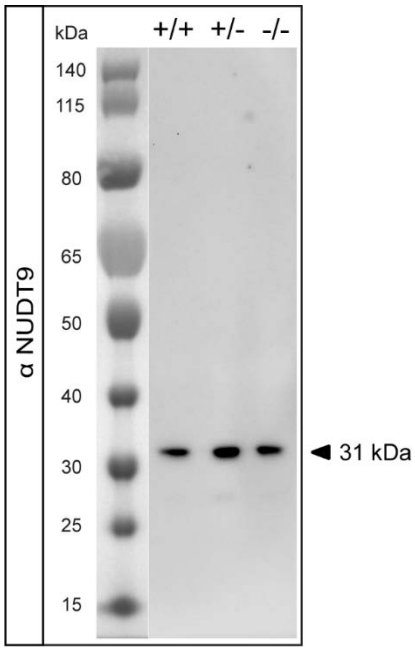

Fig. S1. An orthologue of the human NUDT9 enzyme is expressed in wildtype as well as heterozygous and homozygous NvTRPM2^{1016Stop} animals of *Nematostella*. The NUDT9 expression in total cell lysates was analysed with adult individuals of *Nematostella* using SDS-PAGE gel electrophoresis and Western blot analysis. Parts of the head and foot of wildtype (+/+), heterozygous (+/-) and homozygous (-/-) NvTRPM2^{1016Stop} animals were dissected and lysed. The same single protein band which corresponds to a protein mass of 31 kDa was detected using a commercially available anti-human NUDT9 antiserum in all three different genotypes examined. Three independent experiments gave similar results.

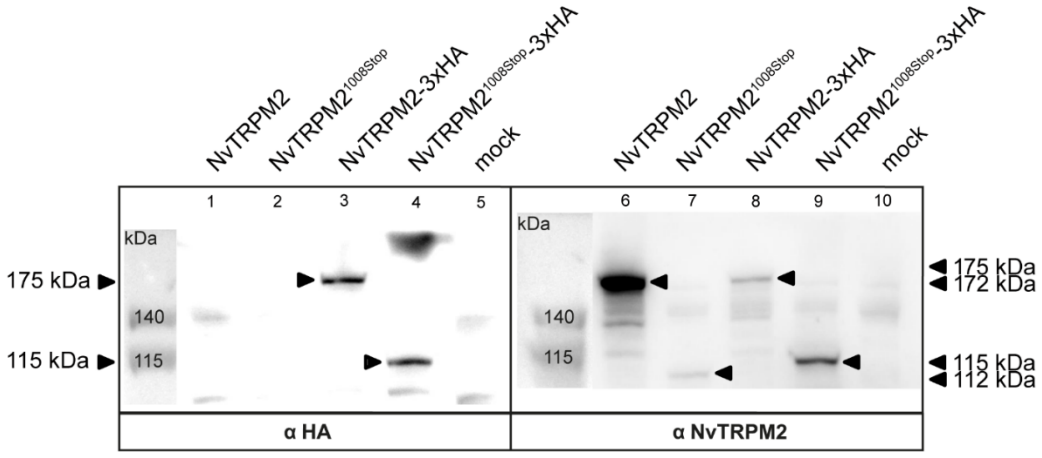

Fig. S2. Total expression of NvTRPM2 and NvTRPM2^{1008Stop} channels in HEK-293 cells. Lysates of cells, heterologously expressing wild-type NvTRPM2 or NvTRPM2^{1008Stop} either with or without 3x-HA tag, were analysed by SDS-PAGE gel electrophoresis and Western blot analysis. Mock-transfected cells were used as negative control. Screening with anti-HA-antiserum (left panel) revealed bands (NvTRPM2-3xHA: 175 kDa, NvTRPM2^{1008Stop}-3xHA: 115 kDA) only in cell lysates with 3xHA-tagged channel variants. Screening with anti-NvTRPM2-antiserum (right panel) both revealed bands (NvTRPM2: 172 kDa, NvTRPM2^{1008Stop}: 112 kDA) in cell lysates with the untagged channel variants and bands (NvTRPM2-3xHA: 175 kDa, NvTRPM2^{1008Stop}-3xHA: 115 kDA) in cell lysates with 3xHA-tagged channel variants.

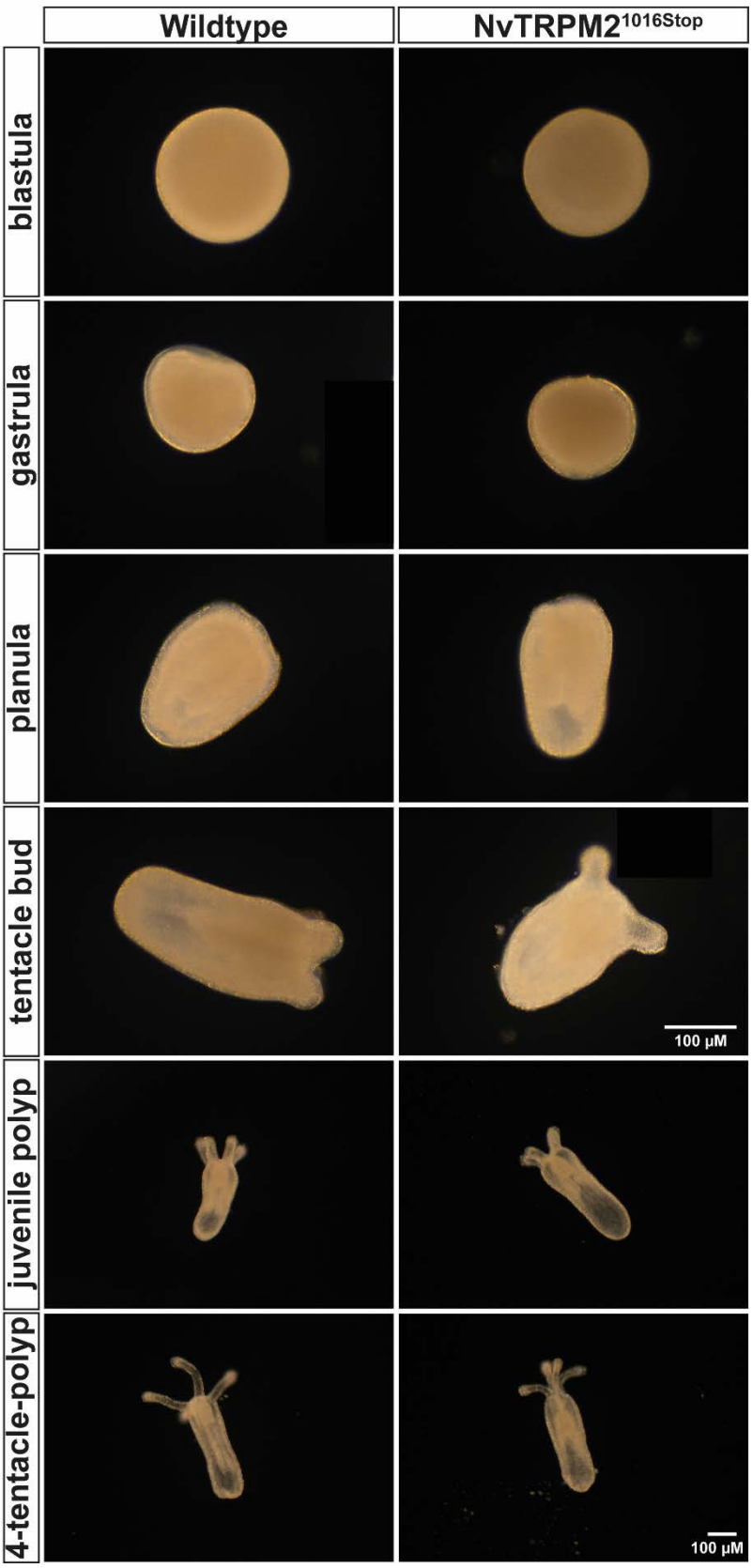

Fig. S3. Comparison of the phenotypes of different developmental stages of wildtype and *NvTRPM2*^{1016Stop} animals. The physical appearance of representative larval stages of both genotypes are shown. No significant differences were found. The upper scale bar applies for the six upper bright-field images, the lower scale bar applies for the four lower bright-field images, both represent 100 µm.